The Chiral Magnetic Effect at Heavy Ion Collisions

Author: Constantijn van der Poel
Supervisor: Umut Gürsoy

A thesis presented for the degree of
Bachelor of Science

Institute for Theoretical Physics
Utrecht University
The Netherlands
15 June 2016

Abstract

Quark-Gluon plasma produced in heavy ion collisions allows for the study of exotic physical effects, one example being the chiral magnetic effect. The generation of electrical current along the magnetic field creates new effects that can be investigated using electrodynamic and hydrodynamic techniques. The dependence of the flow parameters on the "chiral conductivity" is a topic for further analysis, and a framework is presented to investigate this.

Contents

Chapter 1

Background Theory

1.1 Quark-Gluon Plasma

This paper is chiefly concerned with quark-gluon plasma, which is currently a hot topic in theoretical physics (see [6],[11],[17],[24],[25],[26],[27]). Quarks are fundamental particles of matter (see Figure 1.3); for example, they make up protons (2 up and 1 down) and neutrons (2 down and 1 up). The interactions between quarks are chiefly mediated by gluons, the gauge particles responsible for the strong force. The theory describing these phenomena is quantum chromodynamics (QCD). The "chromo" refers to a property of quarks called "color". Quark color is analogous to electrical charge (positive-negative), except there are three opposite pairs (red-antired, green-antigreen, and blue-antiblue; the anticolors are often denoted respectively by magenta, cyan, and yellow) instead of the single pair from electrodynamics.

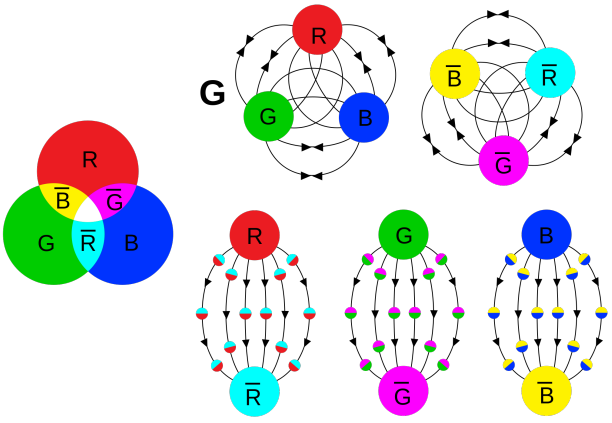

Figure 1.1: Quark Color and Hadron Groupings https://upload.wikimedia.org/wikipedia/commons/thumb/4/41/Qcd_fields_field_(physics).svg/2000px-Qcd_fields_field_(physics).svg.png

Generally, quarks are found in groups (called hadrons): in quark-antiquark pairs (mesons) or triplets (baryons). It is important to note that hadrons are always "color neutral". A meson will have a color-anticolor pair, while a baryon will be red-green-blue or anti(red-green-blue). In fact, a solitary quark has never been observed. The energy required to separate quarks is quite large; so large that the energy barrier to create a new quark-antiquark pair is reached before a quark can be freed. This is known as quark confinement. However, it is possible to loosen the

bonds between quarks. At high temperatures, the quarks can flow freely amongst each other; the critical temperature at which this occurs is roughly 170 MeV. At this temperature, the system crosses over into what is known as the quark-gluon plasma (QGP).

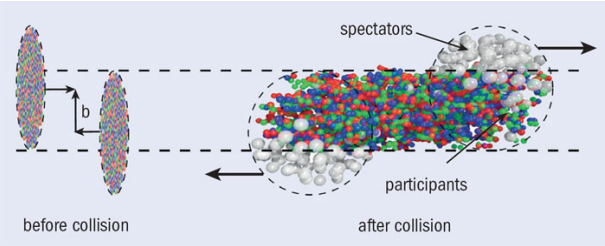

Figure 1.2: Heavy Ion Collision `http://images.iop.org/objects/ccr/cern/53/4/18/CCfir5_04_13.jpg`

However, as time progresses the plasma expands and cools, the quarks re"condense" into hadronic matter: this process is called hadronization. The interactions of quarks is but part of a larger picture, referred to as the Standard Model of Particle Physics.

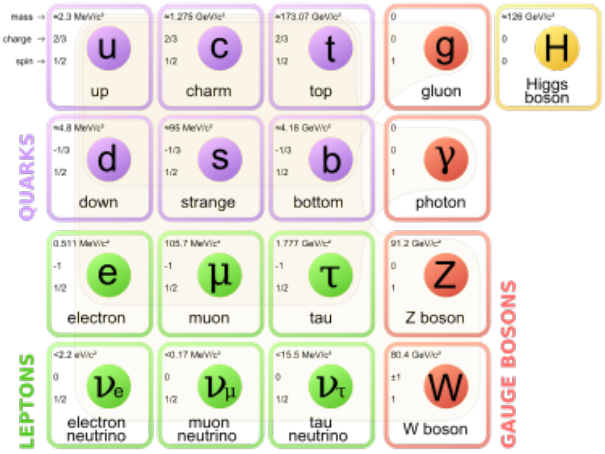

Figure 1.3: Standard Model of Elementary Particles `https://commons.wikimedia.org/w/index.php?curid=4286964`

1.1.1 Why Is QGP Important to Study?

Quark-Gluon plasma can be studied experimentally using heavy ion collisions. This is done at places such as the Relativistic Heavy Ion Collider (RHIC) in New York, the United States, and the Large Hadron Collider (LHC) in Geneva, Switzerland. These colossal machines accelerate nuclei (gold at RHIC, lead at LHC) to near luminal velocities and collide them to probe physics on the smallest scales available to modern science. Heavy ion collisions are able to create the conditions necessary for QGP to exist, albeit for an incredibly short time (the order of femtoseconds)! These ions rarely collide perfectly. As stated earlier, the QGP behaves like a fluid; off-center collisions create a range of interesting flows that will be the topic of interest in this thesis. There is strong coupling between the particles of QGP; as a result the best tool to model such a substance will be hydrodynamics. This will be further

discussed in Chapter 4. Furthermore, it is believed that soon after the Big Bang, the Universe was in a QGP phase, making understanding of this state of matter essential in the study of the early Universe.

1.1.2 Heavy Ion Collisions

Coordinates

Here, we will outline the coordinates used to describe the collision. The axes are oriented as in Figure 1.4:

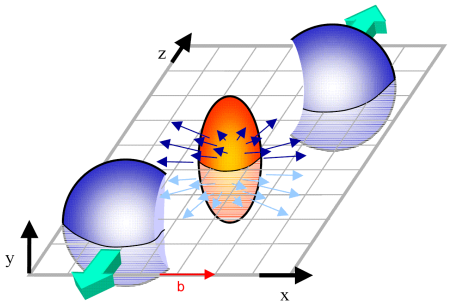

Figure 1.4: Collision Geometry `https://inspirehep.net/record/878251/files/CollisionGeom.png`

The z-axis is oriented along the beam, while the xy-plane, referred to as the transverse plane, has the x-axis oriented along the centers of the nuclei. The impact parameter, b, denotes the distance between the centers of the two nuclei. This determines the "centrality" of the collision, which plays a key role in how the flow of the QGP develops. The particles which are not part of the collision (blue in Figure 1.4) are called spectators; the interacting particles (orange) are called participants. Throughout this paper, we shall make use of the coordinate system conventionally used in the physics of particle collisions. This system reflects the detector layout. For example, since the tranverse momentum is completely determined by the dynamics of the system, it contains valuable information on the inner workings of a collision. They are related to Cartesian spacetime coordinates as follows:

$$\begin{aligned} t &= \tau\cosh(\eta) & \tau &= \sqrt{t^2 - z^2} \\ x &= x_\perp\cos(\phi) & \eta &= \operatorname{arctanh}\left(\frac{z}{t}\right) \\ y &= x_\perp\sin(\phi) & x_\perp &= \sqrt{x^2 + y^2} \\ z &= \tau\sinh(\eta) & \phi &= \arctan\left(\frac{y}{x}\right) \\ v &= \tanh(Y) & Y &= \operatorname{arctanh}\left(\frac{v_z}{c}\right) \end{aligned} \tag{1.1.1}$$

Here, τ is the proper time, η is called the pseudorapidity (which describes angle relative to the beam axis), and Y is the rapidity (which is similar to the particle's speed). The electromagnetic fields derived in Chapter 2 will be cast into this coordinate system, as will the hydrodynamic flow in Chapter 4. The hadron spectrum will also be decomposed using the four-momentum in this new coordinate system, but more on that will follow.

Lorentz Contraction

It is important to note that the particles in the colliders are given a considerable amount of energy, and travel near the speed of light. Special relativity tells us that, as a result, the ions are very Lorentz-contracted in the direction of travel, in the laboratory frame.

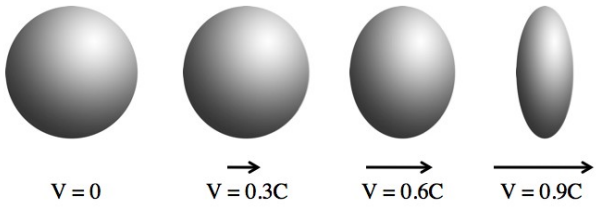

Figure 1.5: Lorentz Contraction http://www.askamathematician.com/wp-content/uploads/2011/01/tallball.jpg

The Lorentz contraction means that the duration of the collision is shorter than the rest-radius of the nucleus divided by the speed of light. As a result, directly after the collision, most of the evolution of the system happens along the beam, and the system can be considered static in the transverse direction (see [22]).

1.2 The Chiral Magnetic Effect

We have now discussed some of the physics regarding quark-gluon plasma, at least on a qualitative level. The high energy levels and strong coupling allow for some exotic physical effects. One that is at the core of this thesis, the chiral magnetic effect (CME), will be further elaborated in this section. The following review was made consulting [1] and [19].

1.2.1 Helicity

First, let us examine helicity, which is defined for a particle with momentum, $\vec{p}$, and spin, $\vec{s}$, as:

$$h = \frac{2\vec{s}\cdot\vec{p}}{p}$$

The eigenvalues of the helicity are ± 1, where the eigenstate with eigenvalue -1 is called "left-helical", and the eigenstate with eigenvalue $+1$ "right-helical". Note that convention has an antiquark have the opposite helicity to its respective quark.

Helicity is rotationally invariant, but it is not invariant under boosts. This is usually shown via the following example. Imagine a fermion with spin and momentum in the z-direction. Its helicity is then $+1$. Now consider another observer, also moving in the z-direction, but faster than the aforementioned fermion. The spin is unchanged in the new frame, however, the fermion now appears to move in the negative z-direction. Now its helicity is -1. Thus, the helicity of a massive fermion

is not invariant under boosts. However, if the fermion is massless, it will be travelling at lightspeed, making it impossible to boost "past" it. Thus, helicity is Lorentz invariant for massless fermions.

1.2.2 Chirality

Chirality is closely related to helicity. Indeed, for a massless particle, it is the same. However, chirality is a more abstract property of a particle, based on how it behaves under certain symmetry transformations, closely associated with the eigenvalues of the matrix γ^5. First, we will examine the four general gamma matrices (also called the Dirac matrices), which are defined by the anticommutator relations: $\{\gamma^\mu, \gamma^\nu\} = 2\eta^{\mu\nu}$. Note that γ^5 is not one of these gamma matrices (it must satisfy different conditions, as we shall see); the index, 5, is a historical artifact, since γ^0 used to be referred to as γ^4. For our purposes, we shall use the chiral representation, where the four gamma matrices are explicitly given by the following 4x4 matrices:

$$\gamma^0 = \begin{pmatrix} 0 & I_2 \\ I_2 & 0 \end{pmatrix} \qquad \gamma^j = \begin{pmatrix} 0 & \sigma^j \\ -\sigma^j & 0 \end{pmatrix}$$

with I_2 the two-dimensional matrix identity and σ^j the Pauli spin matrices:

$$\sigma^1 = \begin{pmatrix} 0 & 1 \\ 1 & 0 \end{pmatrix} \qquad \sigma^2 = \begin{pmatrix} 0 & -i \\ i & 0 \end{pmatrix} \qquad \sigma^3 = \begin{pmatrix} 1 & 0 \\ 0 & -1 \end{pmatrix}$$

We can now discuss the "fifth" gamma matrix, which is defined to satisfy $\{\gamma^5, \gamma^\mu\} = 0$. Furthermore, due to invariance under an overall factor, we have the freedom to impose:

$$\gamma_5^\dagger = \gamma_5 \qquad\qquad (\gamma_5)^2 = 1$$

This will be important to define the chiral projectors. In our representation, γ^5 can be written as:

$$\gamma^5 = i\gamma^0\gamma^1\gamma^2\gamma^3 = \begin{pmatrix} -I_2 & 0 \\ 0 & I_2 \end{pmatrix}$$

Bringing this all together, we can define the projector $P_\pm = \frac{1}{2}(1 \pm \gamma^5)$. With this notation, we can delve into the action for a massive fermion; to describe it, we have the wave function, ψ, which is a complex four-vector. The action is:

$$S = \int \mathrm{d}^4x\, \overline{\psi}(i\partial\!\!\!/ - m)\psi$$

Here, the Dirac adjoint is $\overline{\psi} = \psi^\dagger\gamma^0$ and the Feynman slash denotes $\partial\!\!\!/ = \gamma^\mu\partial_\mu$. Also note that we are using natural units, where $c = \hbar = 1$. As desired, the condition of stationary action, $\frac{\delta S}{\delta\overline{\psi}} = 0$, yields the Dirac equation of motion:

$$(i\partial\!\!\!/ - m)\psi = 0$$

Bask in its glory. The projectors allow ψ to be split into two parts, which we call left- and right-handed chiralities, where $\psi_L = P_-\psi$ and $\psi_R = P_+\psi$. Note that

$P_+\psi_L = P_-\psi_R = 0$. Using the projectors, the action can be decomposed into left- and right-handed terms:

$$S = \int \mathrm{d}^4x \left[i\,\overline{\psi_L}\partial\!\!\!/\psi_L + i\,\overline{\psi_R}\partial\!\!\!/\psi_R - m(\overline{\psi_R}\psi_L + \overline{\psi_L}\psi_R)\right]$$

Note that the mass term "mixes" the chiralities. We shall see that chirality is only conserved for massless fermions.

1.2.3 Axial Symmetry

Symmetries play a large role in modern Physics. Take special relativity, where Lorentz invariance is equivalent to $\mathcal{CPT}$-symmetry. The symmetries are:

- $\mathcal{C}$-symmetry is charge conjugation ($A^\mu \to -A^\mu$ and $\psi \to -i(\overline{\psi}\gamma^0\gamma^2)^T$)
- $\mathcal{P}$-symmetry is parity transformation ($x^j \to -x^j$).
- $\mathcal{T}$-symmetry is time reversal ($x^0 \to -x^0$).

Returning to fermionic theory, when $m = 0$, there is a symmetry of the action under rotations of left- and right-handed fermions in opposite directions:

$$\psi \to e^{i\theta\gamma^5}\psi \qquad\qquad \overline{\psi} \to \overline{\psi}e^{i\theta\gamma^5}$$

Note that since $\{\gamma^5, \gamma^\mu\} = 0$, we can use $\gamma^\mu e^{i\theta\gamma^5} = e^{-i\theta\gamma^5}\gamma^\mu$. Indeed:

$$S \to \int \mathrm{d}^4x\, i\,\overline{\psi}e^{i\theta\gamma^5}\partial_\mu\gamma^\mu e^{i\theta\gamma^5}\psi = \int \mathrm{d}^4x\, i\,\overline{\psi}e^{i\theta\gamma^5}e^{-i\theta\gamma^5}\partial_\mu\gamma^\mu\psi = \int \mathrm{d}^4x\, i\,\overline{\psi}\partial_\mu\gamma^\mu\psi$$

as desired. By Noether's theorem, symmetries of the action yield conservation laws. We can examine the axial current:

$$j_5^\mu = \overline{\psi}\gamma^\mu\gamma^5\psi$$

Rewriting the Dirac equation of motion and its adjoint:

$$\begin{aligned} i\gamma^\mu\partial_\mu\psi - m\psi = 0 &\implies \gamma^\mu\partial_\mu\psi = -im\psi \\ i\partial_\mu\overline{\psi}\gamma^\mu + m\overline{\psi} = 0 &\implies \partial_\mu\overline{\psi}\gamma^\mu = im\overline{\psi} \end{aligned}$$

we can compute the divergence of the axial current:

$$\partial_\mu j_5^\mu = (\partial_\mu\overline{\psi}\gamma^\mu)\gamma^5\psi - \overline{\psi}\gamma^5(\gamma^\mu\partial_\mu\psi) = 2im\overline{\psi}\gamma^5\psi$$

For a classical, massless fermion, the axial current is indeed conserved. However, when quantizing a field theory, processes called "anomalies" emerge, which violate the classical equations of motion.

1.2.4 The ABJ Anomaly

In the case of quantizing fermionic theory, the axial symmetry is broken; this is the Adler-Bell-Jackiw (ABJ) anomaly (also know as the chiral anomaly, see [20]), where chirality is no longer conserved. QCD gauge field configurations can carry topological charge. As explained in [8], this is a special gluon configuration to which a winding number, Q_w, can be assigned, which is topologically invariant.

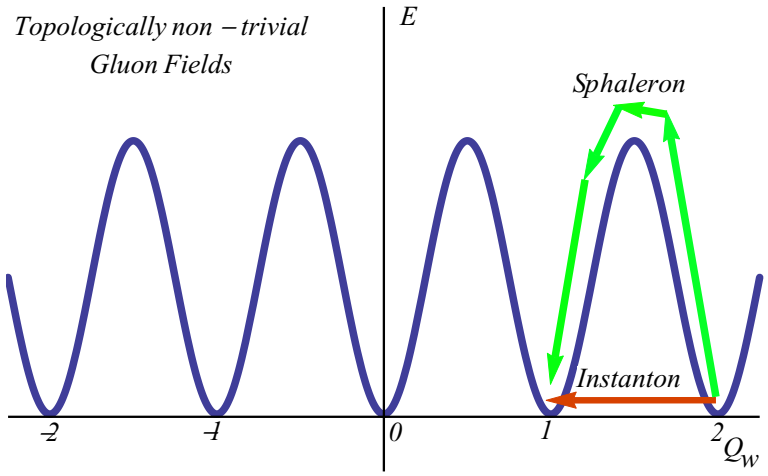

Figure 1.6: Potential Energy as Function of Winding Number

The system can undergo transitions that change its winding number, see Figure 1.6. At low temperatures, there is not enough energy to jump over the potential barrier, so winding number transitions can only occur via tunnelling. These transitions are called instantons. At high temperatures, there is enough energy to jump to a maximum of the potential energy, and the transitions are no longer suppressed. From this point, the system can decay to its original state, but can also decay to an adjacent winding number. Because this transition comes from the decay of an unstable maximum in the potential, it is known as a sphaleron, from the Greek *sphaleros*, meaning slippery (more on sphalerons in [2],[3],[4]). QGP is thus an ideal phase to study these transitions.

Averaged over many transitions, net topological charge is zero. This is due to the fact that there is no explicit $\mathcal{P}$ or $\mathcal{CP}$ breaking in QCD. However, the ABJ anomaly causes the interactions between the quarks and these configurations to locally break $\mathcal{P}$ and $\mathcal{CP}$ parity. This yields fluctuations of topological charge in finite regions of phase space, generating a difference in right- and left-handed particles [12].
To examine the effects of topological charge on handedness more carefully, take the QCD action:

$$S = \int \mathrm{d}^4x \left[\overline{\psi}(i\not{D} - m)\psi - \frac{1}{4}G^a_{\mu\nu}G^{\mu\nu}_a\right] \tag{1.2.1}$$

with $D^\mu = \partial^\mu - igA^\mu$. Here, ψ represents the quark field, and $G^a_{\mu\nu}$ is the gluonic field strength tensor. With the inclusion of nonzero topological charge, another term is added to the QCD action. The ABJ anomaly gives this new topological term as the

spatial integration of the anomalous divergence of the axial current (see [8] or [20]):

$$\frac{\mathrm{d}(N_R - N_L)}{\mathrm{d}t} = \int \mathrm{d}^3x\, \partial_\mu j_5^\mu = -\frac{g^2 N_f}{16\pi^2} \int \mathrm{d}^3x\, G_a^{\mu\nu} \widetilde{G}^a_{\mu\nu} \tag{1.2.2}$$

where $N_{L/R}$ is the number of left-/right-handed particles, N_f is the number of massless quark flavors, and $\widetilde{G}^a_{\mu\nu} = \frac{1}{2}\epsilon_{\mu\nu\lambda\sigma} G^{\lambda\sigma a}$. We can see that this topological term causes the difference in chiralities to change over time, yielding a generation of net chirality.

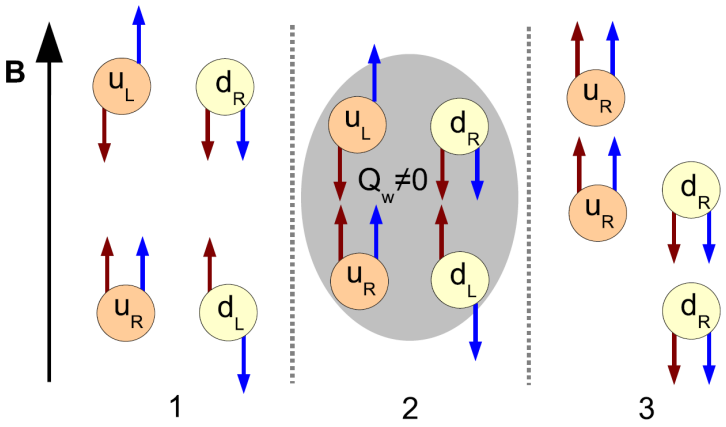

Figure 1.7: The Chiral Magnetic Effect in a large homogeneous magnetic field. The red arrows denote momentum, and the blue arrows denote the spin. The quarks interact with nonzero Q_w (here $Q_w = -1$), switching helicities to right-handed by aligning the momentum with the spin. Source: [11]

Let us examine this qualitatively using Figure 1.7. During a heavy ion collision, strong magnetic fields are present. Additionally, the high temperatures present at the collisions mean we can reasonably neglect the masses of the quarks ([11]), making their chirality the same as their helicity. The quarks will naturally align their magnetic moments with the field, and since they have been assumed to be massless, their momenta will also align along the field. Thus, quarks with opposing helicities will move in opposite directions. Furthermore, since magnetic moment depends on the charge, a quark and antiquark with the same helicity will also move in opposite directions. At time 1 in Figure 1.7, there is an even distribution of helicities. The up quarks with left-handed helicity move oppositely to the up quarks of right-handed helicity, and there is no net current. The same is true for the down quarks. However, at time 2, when the quarks interact with nonzero winding number (in Figure 1.7 $Q_w = -1$), left-handed helical particles become right-handed. Now there is no longer a balance in helicities, and there is a net current generated along the magnetic field at time 3.

In addition to the intrigue of exotic physics, there are also practical applications of the CME. [8] points out that the CME could help to determine whether heavy ion collisions generate quark deconfinement. This is because deconfinement is a necessary requirement for the CME to work; it gives quarks that can separate over distances greater than the radius of a nucleon.

Chapter 2

Electrodynamics

Now that we have set up the system we are examining, as well as the new effect we wish to understand, we will examine how the chiral magnetic effect influences the electromagnetic fields generated by the moving nuclei. The following derivation is based on the work of Eric Marcus' paper on "Magnetohydrodynamics at Heavy Ion Collisions"[16], and is in a sense a continuation of his work. Furthermore, the calculations of the electromagnetic fields of a single particle were completed thanks to the ingenuity of the Chinese team of Li et. al [15].

2.1 Solving the Chiral Maxwell Equations

We wish to describe a charged particle moving in the z-direction through a medium with electrical and magnetic conductivities, σ_E and σ_B. Note that we will work in the regime of $\sigma_E \gg \sigma_B$. We will use the spacetime coordinates: $\vec{x} = (t, \vec{x_\perp}, z)$ and $\vec{x'} = (t', \vec{x_\perp}', z')$. Here, $\vec{x_\perp}$ and $\vec{x_\perp}'$ are respectively the locations in the transverse plane where the field is calculated and where the particle is located.
The Maxwell equations with charge density, $\rho(\vec{x}) = q\,\delta(z - vt)\delta(\vec{x_\perp} - \vec{x_\perp}')$, electric current, $\vec{j}(\vec{x}) = q\,v\,\delta(z - vt)\delta(\vec{x_\perp} - \vec{x_\perp}')\hat{z}$ (note we shall use the notation $\vec{J} = (\rho, \vec{j})$), and chiral magnetic term, $\sigma_B\vec{B}(\vec{x})$, are:

$$\begin{aligned} \vec{\nabla}\cdot\vec{E}(\vec{x}) &= \frac{\rho(\vec{x})}{\epsilon(\omega)} & \vec{\nabla}\cdot\vec{B}(\vec{x}) &= 0 \\ \vec{\nabla}\times\vec{E}(\vec{x}) &= -\partial_t\vec{B}(\vec{x}) & \vec{\nabla}\times\vec{B}(\vec{x}) &= \partial_t\vec{E}(\vec{x}) + \vec{j}(\vec{x}) + \sigma_E\vec{E}(\vec{x}) + \sigma_B\vec{B}(\vec{x}) \end{aligned}$$

Note that we have assumed that the permittivity, $\epsilon(\omega)$, depends on the frequency as $\epsilon(\omega) = 1 + \frac{i\sigma_E}{\omega}$ (as in [15]).
We take the curl of $\vec{\nabla}\times\vec{B}$ and rewrite the equation:

$$\begin{aligned} \vec{\nabla}\times(\vec{\nabla}\times\vec{B}) &= \vec{\nabla}(\vec{\nabla}\cdot\vec{B}) - \vec{\nabla}^2\vec{B} = -\vec{\nabla}^2\vec{B} \\ -\vec{\nabla}^2\vec{B} &= \partial_t(\vec{\nabla}\times\vec{E}) + \vec{\nabla}\times\vec{j} + \sigma_E(\vec{\nabla}\times\vec{E}) + \sigma_B(\vec{\nabla}\times\vec{B}) \\ &= -\partial_t^2\vec{B} + \vec{\nabla}\times\vec{j} - \sigma_E\partial_t\vec{B} + \sigma_B(\vec{\nabla}\times\vec{B}) \end{aligned}$$

Yielding:

$$-\partial_t^2\vec{B} - \sigma_E\partial_t\vec{B} + \vec{\nabla}^2\vec{B} + \sigma_B(\vec{\nabla}\times\vec{B}) = -\vec{\nabla}\times\vec{j}$$

Analogously, for the electric field we have:

$$-\partial_t^2\vec{E} - \sigma_E\partial_t\vec{E} + \vec{\nabla}^2\vec{E} + \sigma_B(\vec{\nabla}\times\vec{E}) = \vec{\nabla}\Big(\frac{\rho}{\epsilon(\omega)}\Big) + \partial_t\vec{j}$$

In general, we have an equation of the form

$$-\partial_t^2\vec{F} - \sigma_E\partial_t\vec{F} + \vec{\nabla}^2\vec{F} + \sigma_B(\vec{\nabla}\times\vec{F}) = \vec{S}$$

where $\vec{S}$ depends on whether the electric or magnetic field is used (this shall be denoted with a subscript). So $\vec{F} = \vec{B} \to S_B(\vec{x}) = -\vec{\nabla}\times\vec{j}$, and $\vec{F} = \vec{E} \to S_E(\vec{x}) = \vec{\nabla}(\frac{\rho}{\epsilon(\omega)}) + \partial_t\vec{j}$. To solve this, we begin by taking the Fourier image of the equation. This is useful because the Fourier image of a derivative takes the form: $\mathscr{F}(\partial_x f) = ik\mathscr{F}(f)$ and $\mathscr{F}(\partial_t f) = -i\omega\mathscr{F}(f)$ (because of the Minkowski metric, whose signature we have chosen to be (-1,1,1,1), the time component picks up a minus sign). For simplicity we rename $\omega^2 + i\sigma_E\omega - \vec{k}^2 = \kappa$. Thus:

$$\kappa\mathscr{F}(\vec{F}) + \sigma_B(i\vec{k}\times\mathscr{F}(\vec{F})) = \mathscr{F}(\vec{S})$$

In matrix form, the equation we wish to solve is:

$$\kappa\begin{pmatrix}\mathscr{F}(F_x)\\ \mathscr{F}(F_y)\\ \mathscr{F}(F_z)\end{pmatrix} + i\sigma_B\begin{pmatrix}k_y\mathscr{F}(F_z) - k_z\mathscr{F}(F_y)\\ k_z\mathscr{F}(F_x) - k_x\mathscr{F}(F_z)\\ k_x\mathscr{F}(F_y) - k_y\mathscr{F}(F_x)\end{pmatrix}$$
$$= \begin{pmatrix}\kappa & -i\sigma_B k_z & i\sigma_B k_y\\ i\sigma_B k_z & \kappa & -i\sigma_B k_x\\ -i\sigma_B k_y & i\sigma_B k_x & \kappa\end{pmatrix}\begin{pmatrix}\mathscr{F}(F_x)\\ \mathscr{F}(F_y)\\ \mathscr{F}(F_z)\end{pmatrix} = \begin{pmatrix}\mathscr{F}(S_x)\\ \mathscr{F}(S_y)\\ \mathscr{F}(S_z)\end{pmatrix}$$

The system is solved to yield:

$$\mathscr{F}(\vec{F}) =$$
$$\begin{pmatrix}(\kappa-\sigma_B k_x)(\kappa+\sigma_B k_x) & \sigma_B(ik_z\kappa - \sigma_B k_x k_y) & -\sigma_B(ik_y\kappa + \sigma_B k_x k_z)\\ -\sigma_B(ik_z\kappa + \sigma_B k_x k_y) & (\kappa-\sigma_B k_y)(\kappa+\sigma_B k_y) & \sigma_B(ik_x\kappa - \sigma_B k_y k_z)\\ \sigma_B(ik_y\kappa - \sigma_B k_x k_z) & -\sigma_B(ik_x\kappa + \sigma_B k_y k_z) & (\kappa-\sigma_B k_z)(\kappa+\sigma_B k_z)\end{pmatrix}\frac{\mathscr{F}(\vec{S})}{\kappa(\kappa^2 - {\sigma_B}^2\vec{k}^2)}$$

2.1.1 Fourier Image

The Fourier image of the the charge density and current are:

$$\mathscr{F}(\rho) = \iiiint e^{i(\omega t - \vec{k}\cdot\vec{x})}q\delta(z-vt)\delta(\vec{x_\perp} - \vec{x_\perp}')\,\mathrm{d}\vec{x}\,\mathrm{d}t = 2\pi q e^{-i\vec{k_\perp}\cdot\vec{x_\perp}'}\delta(\frac{\omega}{v} - k_z)$$
$$\mathscr{F}(\vec{j}) = \iiiint e^{i(\omega t - \vec{k}\cdot\vec{x})}qv\delta(z-vt)\delta(\vec{x_\perp} - \vec{x_\perp}')\hat{z}\,\mathrm{d}\vec{x}\,\mathrm{d}t = 2\pi qv e^{-i\vec{k_\perp}\cdot\vec{x_\perp}'}\delta(\frac{\omega}{v} - k_z)\hat{z}$$

As a result:

$$\mathscr{F}(\vec{S_B}) = -i\vec{k}\times\mathscr{F}(\vec{j}) = -2\pi iqv\,e^{-i\vec{k_\perp}\cdot\vec{x_\perp}'}\delta(\frac{\omega}{v} - k_z)\begin{pmatrix}k_y\\ -k_x\\ 0\end{pmatrix}$$

$$\mathscr{F}(\vec{S_E}) = i\vec{k}\frac{\mathscr{F}(\rho)}{\epsilon(\omega)} - i\omega\mathscr{F}(\vec{j}) = 2\pi iq\omega\,e^{-i\vec{k_\perp}\cdot\vec{x_\perp}'}\delta(\frac{\omega}{v} - k_z)\left[\frac{1}{\omega + i\sigma_E}\begin{pmatrix}k_x\\ k_y\\ k_z\end{pmatrix} - v\hat{z}\right]$$

Finally, we have:

$$\mathscr{F}(\vec{B}) = \frac{-2\pi i q v\, e^{-i\vec{k_\perp}\cdot\vec{x_\perp}'}\delta(\frac{\omega}{v} - k_z)}{\kappa^2 - {\sigma_B}^2\vec{k}^2} \begin{pmatrix} k_y\kappa - i\sigma_B k_x k_z \\ -k_x\kappa - i\sigma_B k_y k_z \\ i\sigma_B {k_\perp}^2 \end{pmatrix}$$

$$\mathscr{F}(\vec{E}) = \frac{2\pi i q\omega\, e^{-i\vec{k_\perp}\cdot\vec{x_\perp}'}\delta(\frac{\omega}{v} - k_z)}{\kappa^2 - {\sigma_B}^2\vec{k}^2} \left[\frac{1}{\kappa}\Big(\frac{\kappa^2 - {\sigma_B}^2\vec{k}^2}{\omega + i\sigma_E} + {\sigma_B}^2 v k_z\Big) \begin{pmatrix} k_x \\ k_y \\ k_z \end{pmatrix} + iv\sigma_B \begin{pmatrix} k_y \\ -k_x \\ \frac{i\kappa}{\sigma_B} \end{pmatrix}\right]$$

As done by [15], the expression for the electric field can be simplified further using charge conservation, $\partial_\mu J^\mu = 0$. The Fourier image of this equation is $-i\omega\mathscr{F}(\rho) + i\vec{k}\cdot\mathscr{F}(\vec{j}) = 0$, which yields the dispersion relation, $\omega = k_z\frac{\mathscr{F}(\vec{j})_z}{\mathscr{F}(\rho)} = k_z v$. Substituting this into the electric field expression yields:

$$\mathscr{F}(\vec{E}) = \frac{2\pi i q\omega\, e^{-i\vec{k_\perp}\cdot\vec{x_\perp}'}\delta(\frac{\omega}{v} - k_z)}{\kappa^2 - {\sigma_B}^2\vec{k}^2} \left[\frac{\kappa + {\sigma_B}^2}{\omega + i\sigma_E} \begin{pmatrix} k_x \\ k_y \\ k_z \end{pmatrix} + iv\sigma_B \begin{pmatrix} k_y \\ -k_x \\ \frac{i\kappa}{\sigma_B} \end{pmatrix}\right]$$

All that remains is to transform the field equations back to position space. However, this shall prove the lengthiest part of the calculation.

2.1.2 Relativistic Limit ($v = 1$)

As an example, we shall calculate the field equations in the relativistic limit. The other calculations follow analogously, and were performed by [15].

Magnetic Field

We shall use as example the y-component; the other components follow analogously, and are thus left as an exercise to the reader. To start, taking the limit $v \to 1$ yields the expression:

$$B_y = \iiiint \frac{\mathrm{d}^3\vec{k}}{(2\pi)^3}\frac{\mathrm{d}\omega}{2\pi}e^{i(\vec{k}\cdot\vec{x} - \omega t)}\frac{-2\pi i q e^{-i\vec{k_\perp}\cdot\vec{x_\perp}'}\delta(\omega - k_z)}{(\omega^2 + i\sigma_E\omega - \vec{k}^2)^2 - \sigma_B\vec{k}^2}(-k_x(\omega^2 + i\sigma_E\omega - \vec{k}^2) - i\sigma_B k_y k_z)$$

We adopt the notation $\vec{b} = \vec{x_\perp} - \vec{x_\perp}'$. The expression is integrated over the entire momentum-space. The k_z integral, using the delta function, evaluates to:

$$B_y = \frac{-iq}{(2\pi)^3}\iint \mathrm{d}^2\vec{k_\perp}\, e^{i\vec{k_\perp}\cdot\vec{b}}\int \mathrm{d}\omega\, \frac{e^{i\omega(z-t)}\big((-i\sigma_E k_x - i\sigma_B k_y)\omega + k_x {k_\perp}^2\big)}{(i\sigma_E\omega - {k_\perp}^2) - {\sigma_B}^2(\omega^2 + {k_\perp}^2)}$$

We switch to cylindrical coordinates, making use of the substitution $\vec{k_\perp} = k_\perp \begin{pmatrix} \cos(\phi) \\ \sin(\phi) \end{pmatrix}$, $\mathrm{d}^2\vec{k_\perp} = k_\perp \mathrm{d}k_\perp \mathrm{d}\phi$, and abbreviating $i\sigma_E\omega - {k_\perp}^2 \to \lambda(\omega, k_\perp)$. Note that, as a result, we have transformed to computing the ϕ-component instead of the y-component. The integral is now:

$$B_\phi = \frac{iq}{(2\pi)^3}\int_0^\infty \mathrm{d}k_\perp\, {k_\perp}^2 \int_{-\infty}^\infty \mathrm{d}\omega\, \frac{e^{i\omega(z-t)}}{\lambda^2(\omega, k_\perp) - {\sigma_B}^2(\omega^2 + {k_\perp}^2)} \int_0^{2\pi} \mathrm{d}\phi\, e^{-ibk_\perp\cos(\phi)}\big(\lambda(\omega, k_\perp)\cos(\phi) + i\sigma_B\omega\sin(\phi)\big)$$

Because $\sin(\phi)e^{-ibk_\perp\cos(\phi)}$ is antisymmetric in ϕ, it integrates to zero. To integrate the cosine term, we use:

$$\int_0^{2\pi} \mathrm{d}\phi\, \cos(\phi)e^{-ibk_\perp\cos(\phi)} = \frac{i}{k_\perp}\int_0^{2\pi}\mathrm{d}\phi\,\frac{\mathrm{d}}{\mathrm{d}b}\Big(e^{-ibk_\perp\cos(\phi)}\Big) = \frac{i}{k_\perp}\frac{\mathrm{d}}{\mathrm{d}b}\Big(2\pi J_0(bk_\perp)\Big) = \frac{2\pi i}{k_\perp}J_1(bk_\perp)$$

With J_0 and J_1 as Bessel functions of the first kind. Thus

$$B_\phi = \frac{q}{(2\pi)^2}\int_0^\infty \mathrm{d}k_\perp\, {k_\perp}^2 J_1(bk_\perp)\int_{-\infty}^{\infty}\mathrm{d}\omega\,\frac{e^{i\omega(z-t)}(i\sigma_E\omega - {k_\perp}^2)}{\lambda^2(\omega,k_\perp) - {\sigma_B}^2(\omega^2+{k_\perp}^2)}$$

To proceed, we must make use of the residue theorem from complex analysis. The denominator is quadratic in ω, so finding the poles is straightforward: $\omega_\pm = \frac{-i\sigma_E{k_\perp}^2 \pm \sigma_B k_\perp\sqrt{{k_\perp}^2-({\sigma_E}^2+{\sigma_B}^2)}}{{\sigma_E}^2+{\sigma_B}^2}$. We will make the assumption $k_\perp \gg \sigma_E, \sigma_B$, which gives the approximation $\omega_\pm \approx \frac{{k_\perp}^2}{i\sigma_E\pm\sigma_B}$ (as done by [15]).
The residues of

$$f(\omega) = \frac{e^{i\omega(z-t)}}{\lambda^2(\omega,k_\perp) - {\sigma_B}^2(\omega^2+{k_\perp}^2)} \approx \frac{e^{i\omega(z-t)}}{-({\sigma_E}^2+{\sigma_B}^2)(\omega-\omega_-)(\omega-\omega_+)}$$

are $\mathrm{Res}\big(f(\omega),\omega_\pm\big) = \mp\frac{e^{i\omega_\mp(z-t)}}{2\sigma_B{k_\perp}^2}$.

According to the residue theorem:

$$\int_C \mathrm{d}\omega\, f(\omega) = 2\pi i\sum_{j=1}^{n}\mathrm{Res}(f,\omega_j)$$

The contour of integration, C, is the semicircle of infinite radius taken in the lower half-plane, since this is where $f(\omega)$ decays to zero. Both poles lie in the lower half plane, yielding:

$$B_\phi = \frac{q}{(2\pi)^2}\int_0^\infty \mathrm{d}k_\perp\, {k_\perp}^2 J_1(bk_\perp)2\pi i\Big[\frac{e^{i\frac{{k_\perp}^2}{i\sigma_E-\sigma_B}(z-t)}}{2(i\sigma_E-\sigma_B)} + \frac{e^{i\frac{{k_\perp}^2}{i\sigma_E+\sigma_B}(z-t)}}{2(i\sigma_E+\sigma_B)}\Big]$$

Finally, we use the integral ([23], 6.631.6),

$$\int_0^\infty \mathrm{d}k_\perp\, {k_\perp}^2 e^{-ia{k_\perp}^2}J_1(bk_\perp) = \frac{-b}{4a^2}e^{i\frac{b^2}{4a}}$$

to yield, after simplifying:

$$\begin{aligned}
B_\phi &= \frac{qi}{4\pi(i\sigma_E-\sigma_B)}\left[\frac{-b(i\sigma_E-\sigma_B)^2}{4(t-z)^2}e^{i\frac{b^2(i\sigma_E-\sigma_B)}{4(t-z)}}\right] + \frac{qi}{4\pi(i\sigma_E+\sigma_B)}\left[\frac{-b(i\sigma_E+\sigma_B)^2}{4(t-z)^2}e^{i\frac{b^2(i\sigma_E+\sigma_B)}{4(t-z)}}\right]\\
&= \frac{qb}{16\pi(t-z)^2}e^{\frac{-\sigma_E b^2}{4(t-z)}}\left[\sigma_E\Big(e^{\frac{i\sigma_B b^2}{4(t-z)}}+e^{\frac{-i\sigma_B b^2}{4(t-z)}}\Big) - i\sigma_B\Big(e^{\frac{i\sigma_B b^2}{4(t-z)}}-e^{\frac{-i\sigma_B b^2}{4(t-z)}}\Big)\right]\\
&= \frac{qb}{16\pi(t-z)^2}e^{\frac{-\sigma_E b^2}{4(t-z)}}\left[\sigma_E\Big(2\cos\big(\frac{\sigma_B b^2}{4(t-z)}\big)\Big) - i\sigma_B\Big(2i\sin\big(\frac{\sigma_B b^2}{4(t-z)}\big)\Big)\right]\\
&= \frac{qb}{8\pi(t-z)^2}e^{\frac{-\sigma_E b^2}{4(t-z)}}\left[\sigma_E\cos\Big(\frac{\sigma_B b^2}{4(t-z)}\Big) + \sigma_B\sin\Big(\frac{\sigma_B b^2}{4(t-z)}\Big)\right]
\end{aligned}$$

An analogous process yields the other components. Note, the $k_\perp$ integral form used to find the z-component is (again using [23], 6.631.6),

$$\int_0^\infty \mathrm{d}k_\perp \, k_\perp \, e^{-ia{k_\perp}^2} J_0(bk_\perp) = \frac{-i}{2a} e^{i\frac{b^2}{4a}}$$

With $b = |\vec{x_\perp} - \vec{x_\perp}'| = \sqrt{{x_\perp}^2 + {x'_\perp}^2 - 2x_\perp x'_\perp \cos(\phi - \phi')}$, and introducing the electromagnetic coupling constant, $\alpha_{\mathrm{em}} = \frac{q^2}{4\pi}$:

$$\begin{aligned}
q\,B_r &= \frac{\alpha_{\mathrm{em}}\, b}{2(t-z)^2} e^{\frac{-\sigma_E\, b^2}{4(t-z)}} \left[\sigma_E \sin\left(\frac{\sigma_B\, b^2}{4(t-z)}\right) - \sigma_B \cos\left(\frac{\sigma_B\, b^2}{4(t-z)}\right)\right] \\
q\,B_\phi &= \frac{\alpha_{\mathrm{em}}\, b}{2(t-z)^2} e^{\frac{-\sigma_E\, b^2}{4(t-z)}} \left[\sigma_E \cos\left(\frac{\sigma_B\, b^2}{4(t-z)}\right) + \sigma_B \sin\left(\frac{\sigma_B\, b^2}{4(t-z)}\right)\right] \\
q\,B_z &= \frac{\alpha_{\mathrm{em}}}{(t-z)} e^{\frac{-\sigma_E\, b^2}{4(t-z)}} \left[\sigma_E \sin\left(\frac{\sigma_B\, b^2}{4(t-z)}\right) - \sigma_B \cos\left(\frac{\sigma_B\, b^2}{4(t-z)}\right)\right]
\end{aligned}$$

Indeed, these are the same field expressions found in [15].

2.2 Electromagnetic Fields of a Point Source

The remaining fields have been derived by Li et al.[15], in an analogous manner to the derivation presented above.

2.2.1 Relativistic Electric Field

As stated in [15], the electric field can only be given analytically in the relativistic limit ($v \to 1$):

$$\begin{aligned}
q\,E_r &= \alpha_{\mathrm{em}} \left[\frac{\gamma\, b}{\Delta^{3/2}}\left(1 + \frac{\sigma_E v\gamma}{2}\sqrt{\Delta}\right) - \frac{\sigma_E e^{-\sigma_E\left(t-\frac{z}{v}\right)}}{v\, b}\left(1 + \frac{\gamma(vt-z)}{\sqrt{\Delta}}\right)\right] e^A \\
q\,E_\phi &= \sigma_B \frac{\alpha_{\mathrm{em}} v^2 \gamma^2\, b}{\Delta^{3/2}}\left[\gamma(vt-z) + A\sqrt{\Delta}\right] e^A \\
q\,E_z &= \alpha_{\mathrm{em}} \left[-\frac{e^A}{\Delta^{3/2}}\left(\gamma(vt-z) + A\sqrt{\Delta} + \frac{\sigma_E \gamma}{v}\Delta\right) + \frac{{\sigma_E}^2}{v^2} e^{-\sigma_E\left(t-\frac{z}{v}\right)} \Gamma(0, -A)\right]
\end{aligned} \tag{2.2.1}$$

where $\Delta = \gamma^2(vt-z)^2 + {x_\perp}^2 + {x'_\perp}^2 - 2x_\perp x'_\perp \cos(\phi - \phi')$, $A = \frac{\sigma_E v\gamma}{2}\left(\gamma(vt-z) - \sqrt{\Delta}\right)$, and $\Gamma(a,z) = \int_z^\infty \mathrm{d}t\, t^{a-1} e^{-t}$ (the incomplete gamma function).

For our purposes, we wish to have the field in particle physics coordinates (described in Section 1.1.2). We shall only be examining the spectator contribution, since the participants contribute at most 10% of the field, and often much less [10]. Since spectators do not participate in the collision, their rapidity does not change, and we take an average beam rapidity of $Y_0 \simeq 8.0$. Additionally, we wish to express the

field in Cartesian components. We can do this using the following transformation:

$$
\begin{aligned}
E_x &= (\cos(\phi) - \cos(\phi'))E_r - (\sin(\phi) - \sin(\phi'))E_\phi \\
E_y &= (\sin(\phi) - \sin(\phi'))E_r - (\cos(\phi) - \cos(\phi'))E_\phi \\
E_z &= E_z
\end{aligned}
$$

As a result, the relativistic electric field becomes:

$$
\begin{aligned}
q\,E_x &= \alpha_{\text{em}}\Bigg[(\cos(\phi) - \cos(\phi'))\Big(\frac{\cosh(Y_0)\,b}{\Delta^{3/2}}\big(1 + \frac{\sigma_E \sinh(Y_0)}{2}\sqrt{\Delta}\big) - \frac{\sigma_E\, e^a}{\tanh(Y_0)\,b}\big(1 + \frac{\tau\sinh(Y_0 - \eta)}{\sqrt{\Delta}}\big)\Big) \\
&\quad - \frac{\sigma_B}{2}(\sin(\phi) - \sin(\phi'))\frac{\sinh^2(Y_0)\,b}{\Delta^{3/2}}\Big(\tau\sinh(Y_0 - \eta) + A\sqrt{\Delta}\Big)\Bigg]e^A \\
q\,E_y &= \alpha_{\text{em}}\Bigg[(\sin(\phi) - \sin(\phi'))\Big(\frac{\cosh(Y_0)\,b}{\Delta^{3/2}}\big(1 + \frac{\sigma_E \sinh(Y_0)}{2}\sqrt{\Delta}\big) - \frac{\sigma_E\, e^a}{\tanh(Y_0)\,b}\big(1 + \frac{\tau\sinh(Y_0 - \eta)}{\sqrt{\Delta}}\big)\Big) \\
&\quad + \frac{\sigma_B}{2}(\cos(\phi) - \cos(\phi'))\frac{\sinh^2(Y_0)\,b}{\Delta^{3/2}}\Big(\tau\sinh(Y_0 - \eta) + A\sqrt{\Delta}\Big)\Bigg]e^A \\
q\,E_z &= \alpha_{\text{em}}\Bigg[\frac{-e^A}{\Delta^{3/2}}\Big(\tau\sinh(Y_0 - \eta) + A\sqrt{\Delta} + \frac{\sigma_E\cosh(Y_0)}{\tanh(Y_0)}\Delta\Big) + \frac{\sigma_E^2\, e^a}{\tanh^2(Y_0)}\Gamma(0, -A)\Bigg]
\end{aligned}
\tag{2.2.2}
$$

where $b = |\vec{x_\perp} - \vec{x_\perp}'|$, $\Delta = \tau^2\sinh^2(Y_0 - \eta) + b^2$, $a = -\sigma_E\,\tau\big(\cosh(\eta) - \frac{\sinh(\eta)}{\tanh(Y_0)}\big)$, $A = \frac{\sigma_E\sinh(Y_0)}{2}\big(\tau\sinh(Y_0 - \eta) - \sqrt{\Delta}\big)$, and $\Gamma(a, z) = \int_z^\infty \mathrm{d}t\, t^{a-1}e^{-t}$ (the incomplete gamma function).

2.2.2 General Magnetic Fields of Point Sources

Magnetic Field

Li et al. give the general magnetic field as:

$$
\begin{aligned}
q\,B_r &= -\sigma_B\alpha_{\text{em}}\frac{v\gamma^2\,b}{\Delta^{3/2}}\Big(\gamma(vt - z) + A\sqrt{\Delta}\Big)e^A \\
q\,B_\phi &= \alpha_{\text{em}}\frac{v\gamma\,b}{\Delta^{3/2}}\Big(1 + \frac{\sigma_E v\gamma}{2}\sqrt{\Delta}\Big)e^A \\
q\,B_z &= \sigma_B\alpha_{\text{em}}\frac{v\gamma}{\Delta^{3/2}}\Bigg(\gamma^2(vt - z)^2\Big(1 + \frac{\sigma_E v\gamma}{2}\sqrt{\Delta}\Big) + \Delta\Big(1 - \frac{\sigma_E v\gamma}{2}\sqrt{\Delta}\Big)\Bigg)e^A
\end{aligned}
$$

The field equations in the form we would like to use are thus:

$$
\begin{aligned}
q\,B_x &= -\alpha_{\rm em}\frac{\sinh(Y_0)\,b}{\Delta^{3/2}}\Bigg(\big(\cos(\phi)-\cos(\phi')\big)\frac{\sigma_B\cosh(Y_0)}{2}\Big(\tau\sinh(Y_0-\eta)+A\sqrt{\Delta}\Big)\\
&\quad+\big(\sin(\phi)-\sin(\phi')\big)\Big(1+\frac{\sigma_E\sinh(Y_0)}{2}\sqrt{\Delta}\Big)\Bigg)e^A\\
q\,B_y &= \alpha_{\rm em}\frac{\sinh(Y_0)\,b}{\Delta^{3/2}}\Bigg(\big(\sin(\phi)-\sin(\phi')\big)\frac{-\sigma_B\cosh(Y_0)}{2}\Big(\tau\sinh(Y_0-\eta)+A\sqrt{\Delta}\Big)\\
&\quad+\big(\cos(\phi)-\cos(\phi')\big)\Big(1+\frac{\sigma_E\sinh(Y_0)}{2}\sqrt{\Delta}\Big)\Bigg)e^A\\
q\,B_z &= \sigma_B\frac{\alpha_{\rm em}}{2}\frac{\sinh(Y_0)}{\Delta^{3/2}}\Bigg(\tau^2\sinh^2(Y_0-\eta)\Big(1+\frac{\sigma_E\sinh(Y_0)}{2}\sqrt{\Delta}\Big)+\Delta\Big(1-\frac{\sigma_E\sinh(Y_0)}{2}\sqrt{\Delta}\Big)\Bigg)e^A
\end{aligned}
\tag{2.2.3}
$$

Chapter 3

Numerics

3.1 Nuclear Integration

The equations derived in Chapter 2 are for a single point source. Since heavy ion collisions are made of many contributing particles, we must integrate over a nucleus made of many point sources. For both spectators and participants, there are two beams (in the $\pm\hat{z}$ direction), meaning $\vec{B}_{\text{total}} = \vec{B}_{\text{s}}^{+} + \vec{B}_{\text{s}}^{-} + \vec{B}_{\text{p}}^{+} + \vec{B}_{\text{p}}^{+}$. Here, the subscript indicates the spectator/participant contribution, and the superscript indicates the beam direction. We shall integrate over a distribution of particles which models the nucleus as a hard sphere of continuously distributed sources. Again, we shall only model the spectator contribution. The hard sphere model is based on the one used in [10].

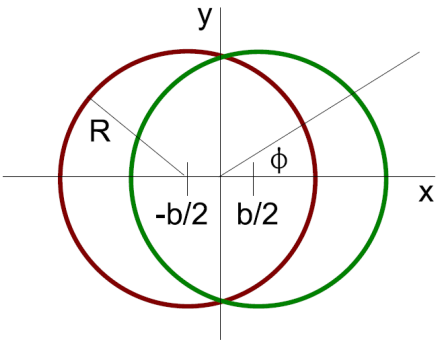

Figure 3.1: Collision Geometry https://inspirehep.net/record/825229/files/tr_plane.png

More specifically, each nucleus is modelled by a sphere with radius, R, and center at $(x, y) = (\pm\frac{b}{2}, 0)$, moving in the z-direction. Keep in mind that the b used here is the impact parameter (see Figure 3.1). We shall examine the probability distribution of finding a particle in the transverse plane. This is given by:

$$\rho_{\pm}(x_{\perp}) = \frac{3}{2\pi}\sqrt{R^2 - \left({x_{\perp}}^2 \pm b\, x_{\perp}\cos(\phi) + \frac{b^2}{4}\right)} \tag{3.1.1}$$

We can simplify the calculation using the symmetry of the spheres:

$$q\,\vec{B}_{\text{total}} = q\,\vec{B}^{+}(\tau, \eta, x_{\perp}, \pi - \phi) + q\,\vec{B}^{+}(\tau, -\eta, x_{\perp}, \phi) \tag{3.1.2}$$

Note that we only need to use ρ_- in the calculation now. The integral over the two crescent-shaped pieces that comprise the spectators is:

$$q\,\vec{B}_s(\tau,\eta,x_\perp,\phi) = -Z\int_{-\frac{\pi}{2}}^{\frac{\pi}{2}} \mathrm{d}\phi' \int_{x_{in}(\phi')}^{x_{\mathrm{out}}(\phi')} \mathrm{d}x'_\perp\, x'_\perp\, \rho_-(x'_\perp) \tag{3.1.3}$$

$$\left(q\,\vec{B}^+(\tau,\eta,x_\perp,\pi-\phi) + q\,\vec{B}^+(\tau,-\eta,x_\perp,\phi)\right) \tag{3.1.4}$$

The values used in our numerical calculations are:

$$\begin{aligned} b &= 7\,\mathrm{fm} \\ R &= 7\,\mathrm{fm} \\ Z &= 82\,p^+ \\ \alpha_{\mathrm{em}} &= \frac{1}{137}\,e^{-2} \\ \sigma_E &= 0.023\,\mathrm{fm}^{-1} \\ Y_0 &= 8.0 \end{aligned}$$

with b the impact parameter, R the radius of the nuclei, Z the charge of the nucleus (equal to the number of protons; in this case we are using lead nuclei), α_{em} the electromagnetic coupling constant, σ_E the electrical conductivity, and Y_0 the average beam rapidity.

3.2 Total Electromagnetic Field

3.2.1 Electromagnetic Field as Function of τ

We can now proceed to compute the integrals numerically. Firstly, we shall examine the τ dependence of the electromagnetic fields for varying values of σ_B.

Magnetic Field

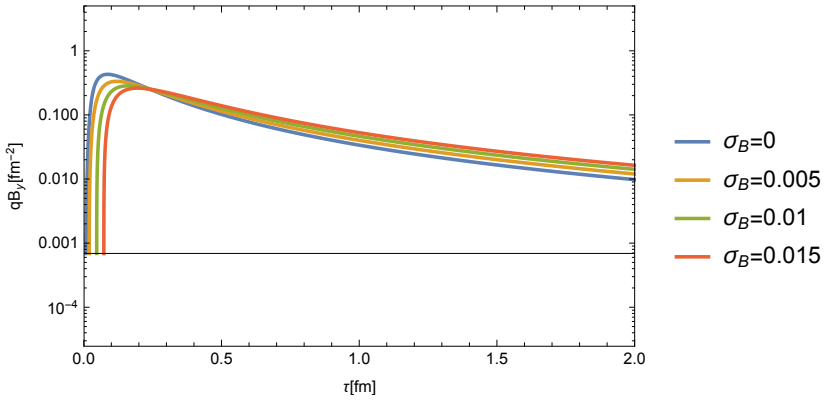

Figure 3.2: $B_y(\tau)$, with $\phi = \frac{\pi}{2}$

For B_y, which is the most significant component of the magnetic field in the absence of the CME [10], the CME causes a delay in the emergence of B_y. Furthermore,

a greater value of σ_B yields a lower maximum, and a lower rate of field strength decay.

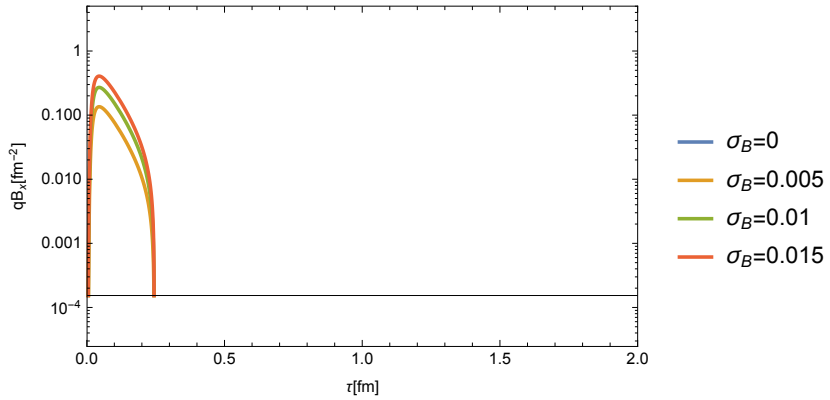

Figure 3.3: $B_x(\tau)$, with $\phi = 0$

In Figure 3.3, we see that the CME causes the magnetic field in the x-direction to reach a greater maximum. The duration of the field's strength is not affected. Note that B_x is zero for $\sigma_B = 0$. If we look at the point-source field expression from Equation 2.2.2, we see that for $\sigma_B = 0$ only the $\sin(\phi) - \sin(\phi')$ term remains. Since this is the x-component, we take $\phi = 0$, leaving only $-\sin(\phi')$. Since $\sin(\phi')$ is integrated from $-\frac{\pi}{2}$ to $\frac{\pi}{2}$, we indeed expect the field component to evaluate to zero.

If we try another value for ϕ, such as $\frac{\pi}{2}$, we find the following:

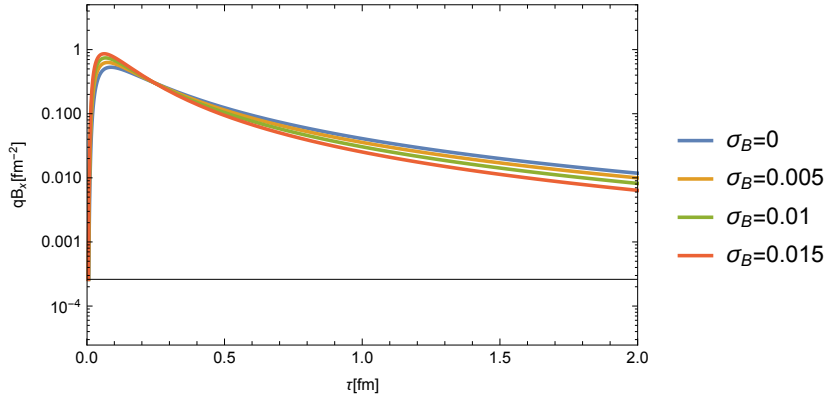

Figure 3.4: $B_x(\tau)$, with $\phi = \frac{\pi}{2}$

As in Figure 3.4, B_x behaves much more similarly to B_y (see Figure 3.2). However, increasing values of σ_B yield the opposite effect as with B_y, causing the field to peak sooner and decay more quickly.

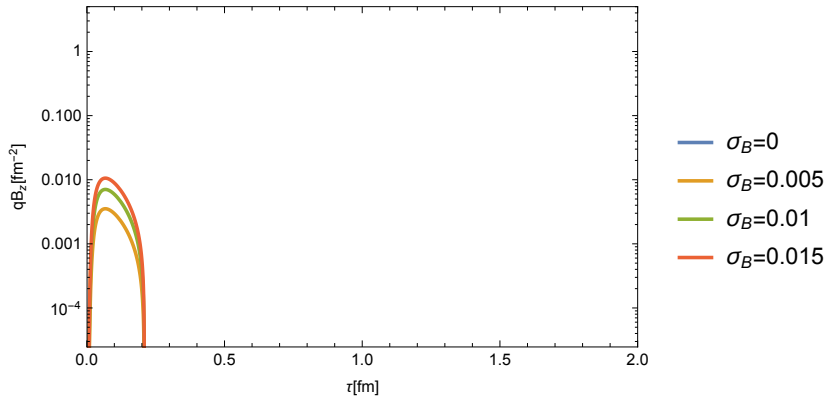

Figure 3.5: $B_z(\tau)$, with $\phi = \frac{\pi}{2}$

With B_z, the influence of the CME is clear: with $\sigma_B = 0$, there is no magnetic field in the z-direction. With the CME present, the z-component behaves similarly to the x-component, although it is weaker in magnitude.

Electric Field

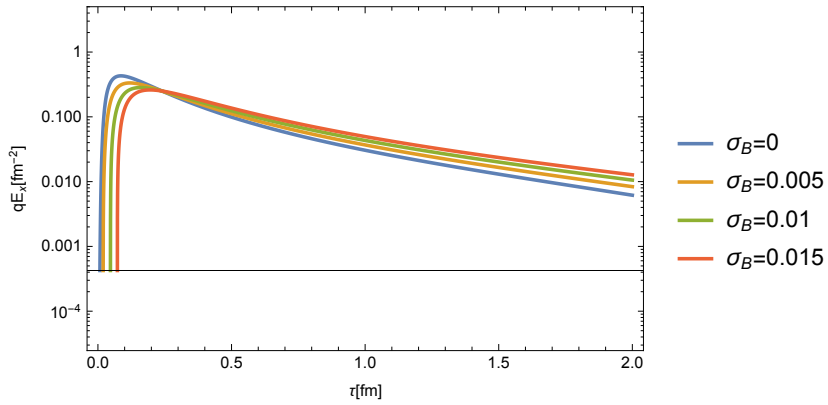

Figure 3.6: $E_x(\tau)$, with $\phi = \frac{\pi}{2}$

With regards to the electric field, E_x is the most significant (see [10]). Here, we see behavior similar to B_y. That is to say, the CME causes a decrease in the field maximum and in its decay.

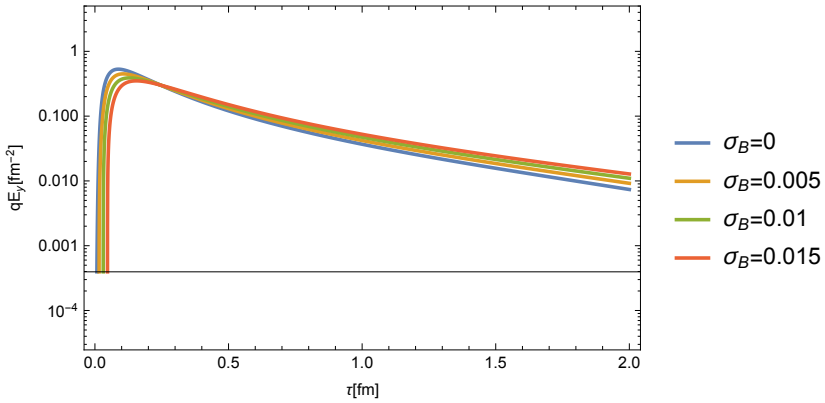

Figure 3.7: $E_y(\tau)$, with $\phi = \frac{3\pi}{2}$

Interestingly, E_y is negative for $\phi = \frac{\pi}{2}$. Thus, to plot its behavior, $\phi = \frac{3\pi}{2}$ was used. E_y responds to σ_B analogously to E_x, however, the shift in the field is less for a given increase in σ_B.

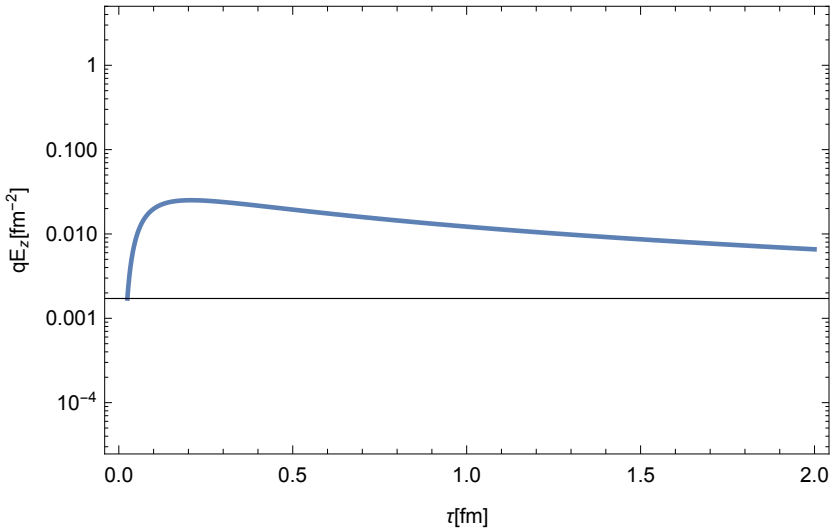

Figure 3.8: $E_z(\tau)$, with $\phi = 0$

The z-component of the electric field is independent of σ_B. It behaves similarly to B_y and B_x, is the sense that there is a sudden spike in the field strength, followed by a gentle decay.

3.2.2 Conclusions

Overall, the chiral magnetic effect has noticeable influence on the total electromagnetic field. For the primary components, B_y and E_x, the CME smooths out the field over time, decreasing the initial surge in strength in favor of a more prolonged field presence. Additionally, the CME introduces a z-component to the magnetic field, as well as strengthens the hitherto less significant B_x and E_y.

Chapter 4

Looking Ahead: Hydrodynamics and Flow Parameters

While the electromagnetic field is a readily observable property of the quark-gluon plasma being studied, it does not reveal the whole picture. Hydrodynamics can be used to calculate the flow of the plasma in the absence of external electromagnetic forces. When this is coupled to the electrodynamics discussed in Chapters 2 and 3, the various flow parameters of the system's hadron momentum spectrum can be approximated. Since these spectra are directly measurable in particle colliders, this theory provides a framework for experimentally testing the validity of the chiral magnetic effect.

In this chapter we shall examine Gubser's flow, an analytic model to describe the dynamics of the expansion of the QGP without the effects of the background electromagnetic field. The result will be a velocity field, u^μ which is a basis for describing the QGP. This will then be used in the Cooper-Frye freeze-out procedure to produce a model for the hadron spectrum of a heavy ion collision. After discussing the model of the hadron spectrum, we shall proceed to discuss how one might couple electromagnetic interactions to the hydrodynamic flow. The goal of this is to yield a velocity field, V^μ, which is the relativistic sum of the velocity due to electromagnetic effects, v^μ, and due to hydrodynamics, u^μ. The total velocity field, V^μ, could then be used to determine the effects of the chiral current on the flow parameters. This is important, as a measurable effect on flow parameters will allow experimenters at heavy ion collisions to more easily determine if the chiral magnetic effect is present.

4.1 Gubser Flow

An early model of hydrodynamic flow in QGP was Bjorken's model, which is based on the assumption of approximate boost invariance (in the beam direction), and translation and rotation invariance (in the transverse plane) [9]. Gubser's solution is a refinement of this model, and is found assuming a finite size plasma produced in a central collision.

In order to move towards a more realistic description of the QGP, Gubser works

with a different set of symmetries; transverse translation invariance, for example, is not a very realistic description of a heavy ion collision. The symmetries are boost invariance (along the beam), rotational invariance (in the transverse plane), and two conformal invariances perpendicular to the beam. The result is a fluid flow that preserves a $SO(1,1) \times SO(3) \times Z_2$ subgroup of the full 4-dimensional conformal group. The Z_2 group comes from invariance under the beam direction, $z \leftrightarrow -z$ (equivalently, $\eta \leftrightarrow -\eta$) [10].

The flow found by Gubser [9] is:

$$u^\tau = \frac{1 + (q\tau)^2 + (qx_\perp)^2}{2q\tau\sqrt{1+g^2}} \tag{4.1.1}$$

$$u^\perp = \frac{qx_\perp}{\sqrt{1+g^2}} \tag{4.1.2}$$

with

$$g = \frac{1 + (qx_\perp)^2 - (q\tau)^2}{2q\tau}$$

Here, q is a constant with dimension $\frac{1}{\text{length}}$, such that the transverse length of the plasma is proportional to $\frac{1}{q}$.

Gubser has also derived an expression for the temperature of the plasma [9]:

$$T = \frac{1}{\tau {f_*}^{1/4}}\left[\frac{\hat{T}_0}{(1+g^2)^{1/3}} + \frac{H_0 g}{\sqrt{1+g^2}}\left(1-(1+g)^{1/6}\right){}_2F_1\left(\frac{1}{2},\frac{1}{6};\frac{3}{2};-g^2\right)\right] \tag{4.1.3}$$

Note that ${}_2F_1$ is a hypergeometric function of the form:

$${}_2F_1\left(\alpha,\beta;\gamma;z\right) = \sum_{n=0}^{\infty}\frac{(\alpha)^n(\beta)^n}{(\gamma)^n}\frac{z^n}{n!}$$

where the rising Pochhammer symbol is used: $(x)^n = x(x+1)...(x+n-1)$. Furthermore, $\hat{T}_0$ is an integration constant which corresponds to the ideal fluid term. f_* relates energy density to temperature via $\epsilon = f_* T^4$. H_0 is a constant which is involved in viscous dissipation. Using conformal invariance, Gubser concludes with:

$$p = \frac{\epsilon}{3}$$
$$\eta = \epsilon^{\frac{3}{4}} H_0$$

with ϵ the energy density and η the shear viscosity. We take $f_* = 11$ and $H_0 = 0.33$ ([5],[9],[14],[18],[21]).

While Gubser flow is certainly an improvement on Bjorken flow, it still has some drawbacks. The most significant is that rotational invariance means that the model can never describe an off-center collision to full detail; nonetheless it can still provide insight into the system's dynamics. According to [10], Gubser's solution yields reasonable results for collisions with an impact parameter of around $7-8$ fm. More accurate results can be obtained via numerical analysis, but this will not be handled here.

4.2 Cooper-Frye Freeze-out

Hydrodynamic theory gives fluid properties such as energy density, fluid velocity, and pressure. However, the detectors used in experimental physics measure other degrees of freedom, such as momentum. Thus, we want a method to connect hydrodynamic theory with kinetic theory. This is known as freeze-out, and occurs when a QGP-phase system cools. As it does, its viscosity increases, rendering a hydrodynamic description invalid. Since this can be quite tricky to model correctly, the process is simplified using a three-dimensional hypersurface, Σ. This has a normal vector, $\mathrm{d}\Sigma_\mu$, which is parameterized as:

$$\mathrm{d}\Sigma_\mu = \epsilon_{\mu\alpha\beta\gamma}\frac{\partial\Sigma^\alpha}{\partial x}\frac{\partial\Sigma^\beta}{\partial y}\frac{\partial\Sigma^\gamma}{\partial z}\mathrm{d}x\,\mathrm{d}y\,\mathrm{d}z \tag{4.2.1}$$

As a starting point, we require the energy-momentum tensors to be equal:

$$T^{\mu\nu}_{\text{kin}} = \int \mathrm{d}\chi\, p^\mu p^\nu f(\vec{p},t,\vec{x}) = T^{\mu\nu}_{\text{hydro}} \tag{4.2.2}$$

Here $f(\vec{p},t,\vec{x})$ represents the particle distribution function from kinetic theory. We shall use the relativistic Boltzmann distribution: $f = \exp(\frac{p^\mu u_\mu}{T_f})$, with T_f the "freeze-out temperature". Using this distribution allows the derivation of an analytic expression. The total number of particles after freeze-out is given by the particle current leaving the hypersurface:

$$N = \int \mathrm{d}\Sigma_\mu n^\mu = \sum_i \int \mathrm{d}^3p \frac{1}{\sqrt{{m_i}^2+\vec{p}^2}}\left(p^0\frac{\mathrm{d}N}{\mathrm{d}^3p}\right)_i \tag{4.2.3}$$

where

$$S_i = \left(p^0\frac{\mathrm{d}N}{\mathrm{d}^3p}\right)_i = \frac{d_i}{(2\pi)^3}\int \mathrm{d}\Sigma_\mu p^\mu f(\vec{p},t,\vec{x}) \qquad d_i = (2s_i+1)(2g_i+1) \tag{4.2.4}$$

Here, 4.2.4 is the Hadron spectrum for the i^{th} species, as derived in [22]. Note that s_i and g_i are the spin and isospin of the i^{th} particle; thus in practice d_i is its degeneracy. With the f as the Boltzmann distribution, the spectrum is:

$$S_i = -\frac{d_i}{(2\pi)^3}\int \mathrm{d}\Sigma_\mu\, p^\mu e^{\frac{p^\mu u_\mu}{T_f}} \tag{4.2.5}$$

To write out the expression for the spectra, we will need to reparameterize the four-momentum:

$$\begin{aligned} p^0 &= m_T\cosh(Y) \\ p^x &= p_T\cos(\phi_p) \\ p^y &= p_T\sin(\phi_p) \\ p^z &= m_T\sinh(Y) \end{aligned} \tag{4.2.6}$$

where we have a "transverse mass": $m_T = \sqrt{{p_T}^2 + {m_i}^2}$. It is important to note that p_T is not the same as $p^\perp$, the perpendicular coordinate of the four-momentum in the transformed system, as will be apparent. The transformed coordinates can be found using $p_\mu = \eta_{\alpha\beta}(\partial_\mu x^\alpha)p^\beta$, resulting in:

$$\begin{aligned} p_\tau &= -m_T \cosh(Y - \eta) \\ p_\eta &= m_T \, \tau \sinh(Y - \eta) \\ p_\perp &= p_T \cos(\phi_p - \phi) \\ p_\phi &= x_\perp \, p_T \sin(\phi_p - \phi) \end{aligned} \tag{4.2.7}$$

In our coordinate system,

$$\mathrm{d}\Sigma_\mu = -\epsilon_{\mu\nu\lambda\rho} \frac{\partial \Sigma^\nu}{\partial \eta} \frac{\partial \Sigma^\lambda}{\partial x_\perp} \frac{\partial \Sigma^\rho}{\partial \phi} \sqrt{-g} \, \mathrm{d}\eta \, \mathrm{d}x_\perp \mathrm{d}\phi \tag{4.2.8}$$

In this equation, $\sqrt{-g}$ is the determinant of the metric we are using, which is $\mathrm{d}s^2 = -\mathrm{d}\tau + \tau^2 \mathrm{d}\eta^2 + {x_\perp}^2 \mathrm{d}\phi^2 + \mathrm{d}{x_\perp}^2$. Thus, $\sqrt{-g} = x_\perp \, \tau_f$. Now we wish to rework the hypersurface area element. To do this, we must make use of:

$$\begin{aligned} \mathrm{d}T &= \frac{\partial T}{\partial x_\perp} \mathrm{d}x_\perp + \frac{\partial T}{\partial \tau} \mathrm{d}\tau = 0 \\ R_f &= -\frac{\partial \tau_f}{\partial x_\perp} = \frac{\partial T / \partial x_\perp}{\partial T / \partial \tau}|_{T_f} \end{aligned}$$

The area element is:

$$\mathrm{d}\Sigma_\mu = (-1, 0, R_f, 0) x_\perp \, \tau_f \, \mathrm{d}\eta \, \mathrm{d}x_\perp \mathrm{d}\phi \tag{4.2.9}$$

Finally, our formula for the hadron spectrum is:

$$S_i = \frac{d_i}{(2\pi)^3} \int_0^{x_f} \mathrm{d}x_\perp \, \tau_f(x_\perp) \int_{-\infty}^{\infty} \mathrm{d}\eta \, e^{-\frac{m_T \, u^\tau}{T_f} \cosh(Y - \eta)} \tag{4.2.10}$$

$$\int_0^{2\pi} \mathrm{d}\phi e^{\frac{p_T \, u^\perp}{T_f} \cos(\phi_p - \phi)} \big(m_T \cosh(Y - \eta) + R_f \, p_T \cos(\phi_p - \phi) \big) \tag{4.2.11}$$

Now, we wish to expand the hadron spectrum in terms of momentum; this is where we will get our flow parameters. The hadron spectrum can thus be rewritten using a Fourier decomposition [13]:

$$\begin{aligned} S_i &= \left(p^0 \frac{\mathrm{d}^3 N}{\mathrm{d}^3 p} \right)_i = \frac{\mathrm{d}^3 N_i}{p_T \, \mathrm{d}p_T \, \mathrm{d}Y \, \mathrm{d}\phi_p} \\ &= \frac{1}{2\pi} \frac{\mathrm{d}^2 N}{p_T \, \mathrm{d}p_T \, \mathrm{d}Y} \left(1 + 2 \sum_{n=1}^{\infty} v_n \cos\big(n(\phi_p - \Psi_R) \big) \right) \\ &= v_0 \big(1 + 2 v_1 \cos(\phi_p - \pi) + 2 v_2 cos(2\phi_p) + ... \big) \end{aligned} \tag{4.2.12}$$

where Ψ_R is the reaction plane angle. The parameters, v_j, are called the flow parameters. v_1 represents direct flow, v_2 represents elliptic flow, then triangular flow, and so forth.

4.2.1 The Pure Flow Parameter: v_0

Without an external electromagnetic field, only the v_0 term remains. It turns out that, since $|\vec{v}| \ll |\vec{u}|$, we can use the pure term in higher order flow parameters as well, since hydrodynamics will remain the dominant contributor. This term was already found in [16]:

$$S_i = \frac{\mathrm{d}_i}{2\pi^2} \int \mathrm{d}x_\perp \, \tau(x_\perp) \left[m_T \, \mathrm{K}_1\left(\frac{m_T u^\tau}{T_f}\right) \mathrm{I}_0\left(\frac{p_T u^\perp}{T_f}\right) + R_f \, p_T \, \mathrm{K}_0\left(\frac{m_T u^\tau}{T_f}\right) \mathrm{I}_1\left(\frac{p_T u^\perp}{T_f}\right) \right] \tag{4.2.13}$$

where $\mathrm{d}_i = 2$ is the degeneracy for pions and protons. The spectrum is finalized by choosing the constants q and $\hat{T}_0$, and doing the $x_\perp$ integral numerically. The constants chosen by [16] were $q = \frac{1}{6.4\mathrm{fm}}$ and $\hat{T}_0 = 10.8$.

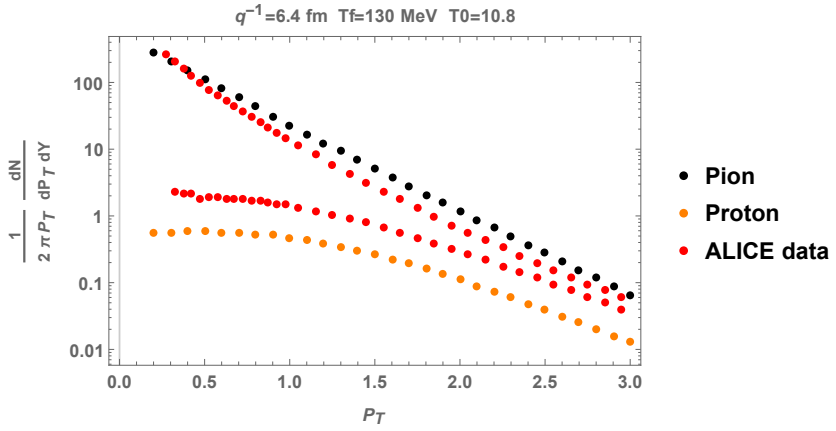

Figure 4.1: Proton and Pion spectra from [16], using data from the ALICE collaboration [7]

4.3 A Proposal for the Electrodynamic Equation of Motion

The Cooper-Frye freezeout procedure has given us a model to derive flow parameters from a velocity field. For a more accurate model, we wish to incorporate both hydrodynamic and electrodynamic flows. To find the electrodynamic flow, we will first need an equation of motion. To start, we must boost to the fluid rest frame, so that only electrodynamic effects are present. The fluid is moving with velocity, $\vec{u}$ from the Gubser model (Equation 4.1), so we will boost with $\Lambda(-\vec{u})$, where in general a boost of $\vec{\beta}$ is given by:

$$\begin{pmatrix} \gamma & -\gamma\beta_x & -\gamma\beta_y & -\gamma\beta_z \\ -\gamma\beta_x & 1+(\gamma-1)\frac{{\beta_x}^2}{\beta^2} & (\gamma-1)\frac{\beta_x\beta_y}{\beta^2} & (\gamma-1)\frac{\beta_x\beta_z}{\beta^2} \\ -\gamma\beta_y & (\gamma-1)\frac{\beta_y\beta_x}{\beta^2} & 1+(\gamma-1)\frac{{\beta_y}^2}{\beta^2} & (\gamma-1)\frac{\beta_y\beta_z}{\beta^2} \\ -\gamma\beta_z & (\gamma-1)\frac{\beta_z\beta_x}{\beta^2} & (\gamma-1)\frac{\beta_z\beta_y}{\beta^2} & 1+(\gamma-1)\frac{{\beta_z}^2}{\beta^2} \end{pmatrix} \tag{4.3.1}$$

Furthermore, the field tensor in the lab frame is:

$$\begin{pmatrix} 0 & -E_x & -E_y & -E_z \\ E_x & 0 & -B_z & B_y \\ E_y & B_z & 0 & -B_x \\ E_z & -B_y & B_x & 0 \end{pmatrix} \tag{4.3.2}$$

Here, the electromagnetic fields are those found in Chapter 3. Combining 4.3.1 and 4.3.2, the electromagnetic field tensor in the fluid rest frame will be given by

$$F'^{\mu\nu} = \Lambda^{\mu}_{\alpha}\Lambda^{\nu}_{\beta}F^{\alpha\beta} \tag{4.3.3}$$

With the electromagnetic fields in the fluid rest frame, we can solve for the electrodynamic flow. The equation of motion is

$$m\partial_t\vec{v}' = q\,\vec{E}' + q\,\vec{v}' \times \vec{B}' - \mu\, m\,\vec{v}' = 0 \tag{4.3.4}$$

Here, the first two terms come from the Lorentz force, while the third term represents the effects of viscous drag.

For further research, we propose the additional term, $q_5\vec{B}$. Here, q_5 is the "axial charge", which can be decomposed into $q_5 = \chi_5\,\mu_5$. χ_5 is the "chiral susceptibility", which can be computed using lattice QCD. μ_5 is the chiral potential discussed in [8] and [12], however, there is yet no theoretical method to calculate this.
The equation to solve is then:

$$m\partial_t\vec{v}' = q\,\vec{E}' + q\,\vec{v}' \times \vec{B}' - \mu\, m\,\vec{v}' + q_5\,\vec{B}' = 0 \tag{4.3.5}$$

This can be solved using straightforward matrix algebra. In matrix form the modified equation of motion is:

$$\begin{pmatrix} -\mu & q\,B_z{}' & -q\,B_y{}' \\ -q\,B_z{}' & -\mu & q\,B_x{}' \\ q\,B_y{}' & -q\,B_x{}' & -\mu \end{pmatrix} \begin{pmatrix} v_x \\ v_y \\ v_z \end{pmatrix} = \begin{pmatrix} -q\,E_x{}' - q_5\,B_x{}' \\ -q\,E_y{}' - q_5\,B_y{}' \\ -q\,E_z{}' - q_5\,B_z{}' \end{pmatrix} \tag{4.3.6}$$

Solving yields:

$$\begin{pmatrix} v_x \\ v_y \\ v_z \end{pmatrix} = \frac{1}{\mu(q^2\vec{B}^2+\mu^2)} \begin{pmatrix} q^2B_x{}'^2+\mu^2 & q^2B_x{}'B_y{}'+q\mu B_z{}' & q^2B_x{}'B_z{}'-q\mu B_y{}' \\ q^2B_x{}'B_y{}'-q\mu B_z{}' & q^2B_y{}'^2+\mu^2 & q^2B_y{}'B_z{}'+q\mu B_x{}' \\ q^2B_x{}'B_z{}'+q\mu B_y{}' & q^2B_y{}'B_z{}'-q\mu B_x{}' & q^2B_z{}'^2+\mu^2 \end{pmatrix} \times \begin{pmatrix} qE_x{}'-q_5B_x{}' \\ qE_y{}'-q_5B_y{}' \\ qE_z{}'-q_5B_z{}' \end{pmatrix} \tag{4.3.7}$$

After solving for $\vec{v}$, we transform it back to the lab frame with $\Lambda(\vec{u})$. Relativistic addition of velocities yields $\vec{V}$, the total flow velocity. Plugging this into the hadron spectrum will allow one to calculate the flow parameters with chiral magnetic effect.

Chapter 5

Conclusions

In this thesis, we have examined the new topic of the chiral magnetic effect, particularly in the context of quark-gluon plasma. The CME is a quantum effect which emerges as a result of nonconservation of chirality in a system due to topological charge transitions. We have delved into how it influences the dynamics of the electromagnetic fields present in heavy ion collisions, and have worked through the solution of the Maxwell equations with an additional chiral current. After running numerical calculations, we were able to see how the CME changes the dynamics of the fields, by "smoothing out" the decay of the most prominent field components, and increasing the magnitude of the remaining components (E_z, however, is unaffected by this new term).

Looking forward to potential additional research to further the theoretical understanding of the CME, we examined how, using hydrodynamics, we might be able to study the influence of the CME on flow parameters. Expressions for these parameters in terms of the chiral conductivity, σ_B, provide an experimental framework with which to measure and test the theories discussed in this thesis. We leave this final topic, the modified electrodynamic equation of motion (with q_5 term) as an open area for further research.

Bibliography

[1] *The dirac equation*, Cambridge Department of Applied Mathematics and Theoretical Physics. `http://www.damtp.cam.ac.uk/user/tong/qft/four.pdf`.

[2] P. Arnold and L. McLerran, *Sphalerons, small fluctuations and baryon number violation in electroweak theory*, (1987).

[3] ——, *The sphaleron strikes back*, (1988).

[4] P. Arnold, D. Son, and L. Yaffe, *The hot baryon violation rate is* $O(\alpha_w^5 T^4)$, (1997).

[5] S. Borsanyi, G. Endrodi, Z. Fodor, A. Jakovac, S. D. Katz, S. Krieg, C. Ratti, and K. K. Szabo, (2010).

[6] W. T. Deng and X. G. Huang, (2012). [arXiv:1201.5108 [nucl-th]].

[7] B. A. et al. [ALICE Collaboration], (2013). [arXiv:1303.0737[hep-ex]].

[8] K. Fukushima, D. E. Kharzeev, and H. J. Warringa, *The chiral magnetic effect*, (2008).

[9] S. S. Gubser, *Symmetry constraints on generalizations of bjorken flow*, (2010).

[10] U. Gürsoy, D. Kharzeev, and K. Rajagopal, *Magnetohydrodynamics, charged currents and directed flow in heavy ion collisions*, (2014).

[11] D. E. Kharzeev, L. D. McLerran, and H. J. Warringa, *The effects of topological charge change in heavy ion collisions: 'event by event $\mathcal{P}$ and $\mathcal{CP}$ violation'*, (2007). [arXiv:0711.0950 [hep-ph]].

[12] D. E. Kharzeev and H. J. Warringa, *Chiral magnetic conductivity*, (2009).

[13] N. v. d. Kolk, *To flow or not to flow: A study of elliptic flow and nonflow in proton-proton collisions in alice*, (2011).

[14] P. Kovtun, D. T. Son, and A. O. Starinets, *Viscosity in strongly interacting quantum field theories from black hole physics*, (2005). [hep-th/0405231].

[15] H. Li, X.-L. Sheng, and Q. Wang, *Electromagnetic fields with electric and chiral magnetic conductivities in heavy ion collisions*, (2016).

[16] E. Marcus, *Magnetohydrodynamics at heavy ion collisions*, (2015).

[17] L. McLerran and V. Skokov. [arXiv:1305.0774 [hep-ph]].

[18] H. B. Meyer, (2007). [arXiv:0704.1801[hep-lat]].

[19] P. B. Pal, *Dirac, majorana and weyl fermions.* Saha Institute of Nuclear Physics, Oct. 2010.

[20] M. Peskin and D. Schroeder, *An Introduction to Quantum Field Theory*, Advanced book classics.

[21] G. Policastro, D. T. Son, and A. O. Starinets, *The shear viscosity of strongly coupled $n = 4$ supersymmetric yang-mills plasma*, (2001). [hep-th/0104066].

[22] P. Romatschke, *New developments in relativistic viscous hydrodynamics*, (2009).

[23] I. M. Ryzhik and I. S. Gradshteyn, *Table of Integrals, Series, and Products*, Academic Press, fifth ed., Jan. 1994.

[24] V. Skokov, A. Y. Illarionov, and V. Toneev, (2009). [arXiv:0907.1396 [nucl-th]].

[25] K. Tuchin, (2011). [arXiv:1006.3051 [nucl-th]].

[26] ——, (2013). [arXiv:1301.0099].

[27] V. Voronyuk, V. D. Toneev, W. Cassing, E. L. Bratkovskaya, V. P. Konchakovski, and S. A. Voloshin, (2011). [arXiv:1103.4239 [nucl-th]].